doi:10.1246/cl.2012.850

Published on the web August 11, 2012

Lithium Insertion–Deinsertion Reactions of Ultrafine SnO_2 Nanoparticles Synthesized by Microwave Heating

Masashi Yoshinaga,† Norihito Kijima,* Sonoko Wakahara, and Junji Akimoto
National Institute of Advanced Industrial Science and Technology (AIST), Tsukuba Central 5, 1-1-1 Higashi, Tsukuba, Ibaraki 305-8565

(Received April 4, 2012; CL-120293; E-mail: n-kijima@aist.go.jp)

Ultrafine SnO_2 nanoparticles were successfully synthesized by microwave heating. The SnO_2 nanoparticles worked as a rechargeable electrode material for a lithium-ion battery. Micro-Raman spectroscopy, X-ray diffraction, and cyclic voltammetry studies of the SnO_2 nanoparticles elucidated that the lithium insertion–deinsertion reactions during the 1st cycle were caused by both redox of SnO_2 and Li–Sn alloying–dealloying reactions. The redox reactions were irreversible and disappeared via charge–discharge cycling, and only the Li–Sn alloying–dealloying reactions took place at the later cycle.

SnO_2 and Sn-based anode materials are promising as alternative materials to carbon anodes for lithium-ion batteries because of a high specific capacity for lithium storage.[1–3] Although a number of studies regarding SnO_2 as well as Sn-based anode materials have been done over the past several years, poor cyclabilities and large irreversible capacities are still problems.

We have recently succeeded in syntheses of ultrafine SnO_2 nanoparticles as well as α-Fe_2O_3 nanoparticles by microwave heating.[4–7] The microwave-synthesized SnO_2 nanoparticles are one of the smallest particles among SnO_2 reported as anode materials. This nanosized SnO_2 showed larger lithium storage capacity than those of large-sized particles, and the cycle performance was improved by the smallness and uniformity of SnO_2.[4,5] However, the electrode reaction mechanism of such ultrafine particles has not been elucidated sufficiently because of difficulty of analysis for nanosized materials.

Raman spectroscopy can identify bonding states of nanosized oxides as well as noncrystalline oxides, although such materials are difficult to be analyzed by laboratory X-ray diffraction (XRD). As far as we know, there has been no previous report of Raman studies of nanosized SnO_2 electrodes under charge–discharge conditions. In this work, the electrodes of microwave-synthesized SnO_2 nanoparticles were intensively analyzed by the Raman spectroscopy as well as XRD under different depth of charge–discharge conditions.

SnO_2 nanoparticles were synthesized by microwave heating. One hundred cubic centimeters of 0.1 mol dm^{-3} $SnCl_4 \cdot 5H_2O$ solution was heated by microwave irradiation (2.45 GHz, 1200 W) for 5 min with stirring. The resulting suspension was washed with distilled water and then freeze-dried. Details of the microwave synthesis has been reported in our previous paper.[4] The XRD pattern of the obtained nanoparticles was indexed as a single phase of tetragonal rutile-type SnO_2.[4]

Transmission electron microscopy (TEM) images of nanoparticles were taken with a JEOL JEM-2010 microscope at an accelerating voltage of 200 kV. Specimens for TEM analysis were prepared by placing a small drop of a sonicated ethanol solution with the SnO_2 nanoparticles onto a porous microgrid supported on a Cu mesh. XRD patterns were obtained on a Rigaku RINT-2550VHF diffractometer with Cu Kα radiation. Micro-Raman spectroscopy was carried out using a Thermo Fisher DXR Raman spectrometer with 532 nm exciting laser radiation. Micro-Raman spectra were collected in the spectral range of 100 to 1200 cm^{-1} with a resolution better than 5 cm^{-1}.

Galvanostatic charge–discharge measurements were conducted at 25 °C with a charge–discharge device (Nagano Co., Ltd., BTS-2004W) in the voltage range of 0.01 to 3.00 V under the current density of 0.2 mA cm^{-2}. Cyclic voltammograms were examined using a Solartron SI 1280B potentiostat/galvanostat with a scan rate of 0.1 mV s^{-1} and a scan range between 0.01 and 3.0 V. The electrolyte was a 1 mol dm^{-3} solution of $LiPF_6$ in blended ethylene carbonate and diethyl carbonate at a volumetric ratio of 1:1. The counter and reference electrodes were Li foil, and the working electrode consisted of active material, acetylene black, and poly(vinylidene fluoride) at a weight ratio of 6:3:1. The working electrode slurry-coated on Cu foil was dried at 80 °C in an argon-filled glove box (−85 °C dew point) before the fabrication of a test cell.

Figure 1 depicts TEM images of the SnO_2 nanoparticles formed by the microwave heating. Most of the primary particles had ellipsoid shapes, and their sizes were around 5 nm, which is in good agreement with the XRD and the N_2 adsorption analyses.[4] As Figure 1a shows, these primary particles connected to each other. This agglomeration would occur when the TEM specimens were dried before the observations. The nanoparticles were highly crystalline because the lattice images were clearly observed, as Figure 1b shows.

Figure 2 shows lithium insertion–deinsertion curves of the microwave-synthesized SnO_2 nanoparticles over the 50 cycles. The initial insertion capacity of 1670 mA h g^{-1} (cutoff voltage: 10 mV) was achieved, and a large irreversible capacity was observed after the 1st cycle, which has been reported by many research groups.[2,4,8] The insertion capacity at the 2nd cycle was 970 mA h g^{-1}, and thereafter the capacity gradually decreased with increasing of cycle numbers. The insertion capacity at the 50th cycle was 644 mA h g^{-1}. The capacity retention was 66% from the 2nd cycle to the 50th cycle, which is higher than those of the commercial product and the conventionally heated specimen.[2,4]

Figure 3 shows cyclic voltammograms of the microwave-synthesized SnO_2 nanoparticles at the 1st cycle and the 50th cycle. In the 1st cycle, broad peaks were detected above 0.5 V, which correspond to the redox reactions ($SnO_2 + 4Li^+ + 4e^- \rightleftarrows Sn + 2Li_2O$).[9] These peaks disappeared at the 50th cycle. This finding indicates that no redox reaction of SnO_2 took place at the 50th cycle. On the other hand, peaks under 0.5 (insertion) and 0.7 V (deinsertion) were observed at both the 1st

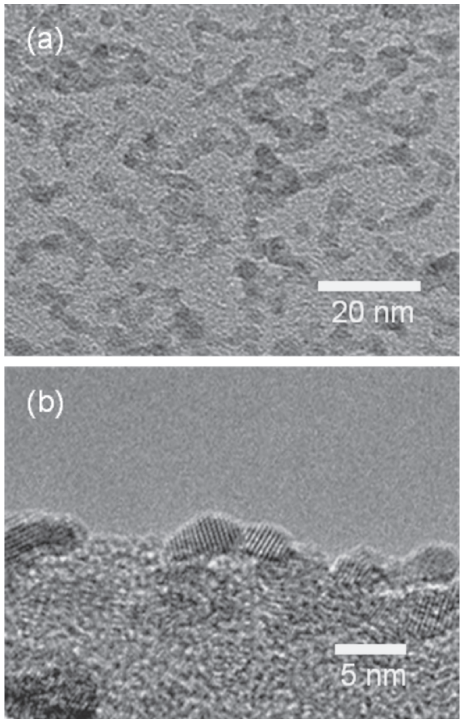

Figure 1. TEM images of the microwave-synthesized SnO_2 nanoparticles (a) on a microgrid and (b) on the edge of a porous microgrid.

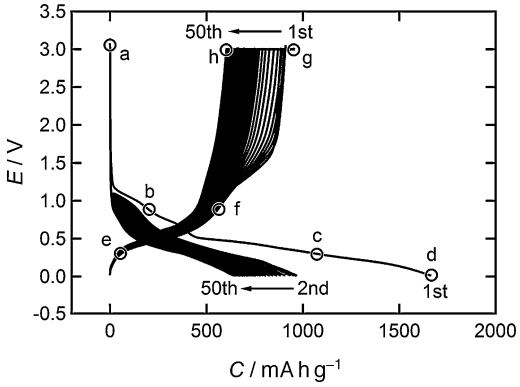

Figure 2. Lithium insertion–deinsertion curves of the microwave-synthesized SnO_2 nanoparticles over the 50 cycles; voltage: 3.0–0.01 V, and current rate: 0.8 mA cm^{-2}. The open circles (○) represent the measurement points of the XRD and Raman analyses at different voltages: (a) open circuit voltage, (b) 0.9, (c) 0.3, (d) 0.01, (e) 0.3, (f) 0.9, and (g) 3.0 V during the 1st cycle, and (h) 3.0 V at the 50th cycle.

and 50th cycles. These peaks were associated with the alloying–dealloying reactions ($Sn + 4.4Li^+ + 4.4e^- \rightleftarrows Li_{4.4}Sn$).[2] As compared with the 1st cycle, the peak currents decreased at the 50th cycle, which suggests the irreversibility of the Li–Sn alloying–dealloying reactions.

Figure 4 presents ex situ XRD patterns of the SnO_2 nanoparticle electrodes. Broad peaks of SnO_2 were observed during the 1st insertion–deinsertion process. The peak intensities of SnO_2 at around 26° decreased gradually during the lithium insertion and increased slightly during the deinsertion. Broad

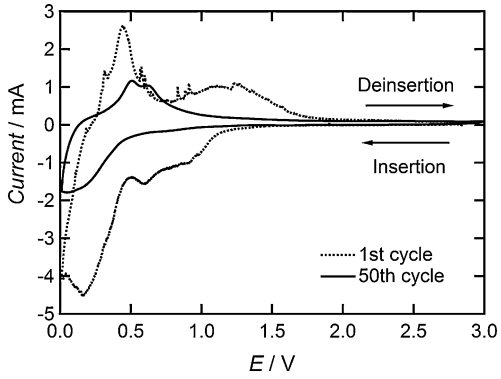

Figure 3. Cyclic voltammograms of the microwave-synthesized SnO_2 nanoparticles for the 1st cycle and the 50th cycle.

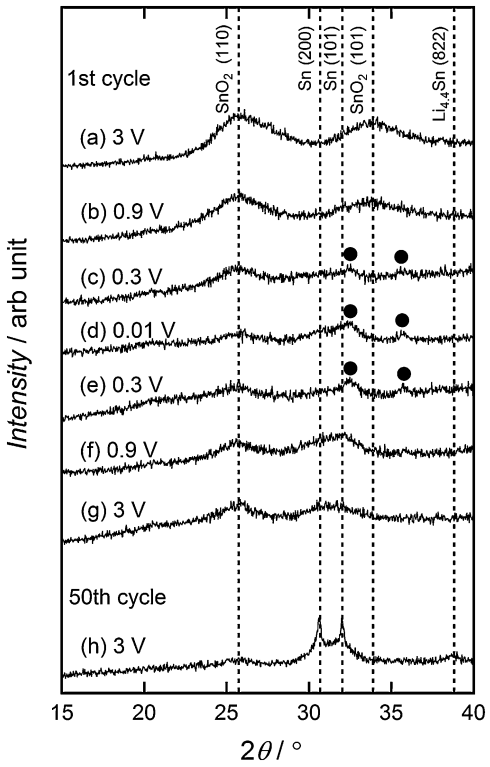

Figure 4. Ex situ XRD patterns of the SnO_2 nanoparticle electrodes at different voltages during the 1st cycle and at the end of 50th cycle. All electrodes were exposed to air before the measurements.

peaks of metal Sn phase were observed at around 30.6 and 32° until the end of the 1st cycle. In addition, two peaks indicated by black circle (●) were also detected at low voltage regions (Figures 4c–4e), which were identified as Li_2SnO_3 and Li_8SnO_6. These compounds would be generated from oxidation of Li–Sn alloy phase because the electrodes were exposed to air before the measurements.

At the 50th cycle (Figure 4h), two peaks of Sn metal phase were obviously detected. The grain size of Sn metal was increased after 50 cycles because of sharpness of the diffraction peaks. The crystallite size of Sn metal was estimated to be about 30 nm from the peak widths of Sn phase at the 50th cycle. A

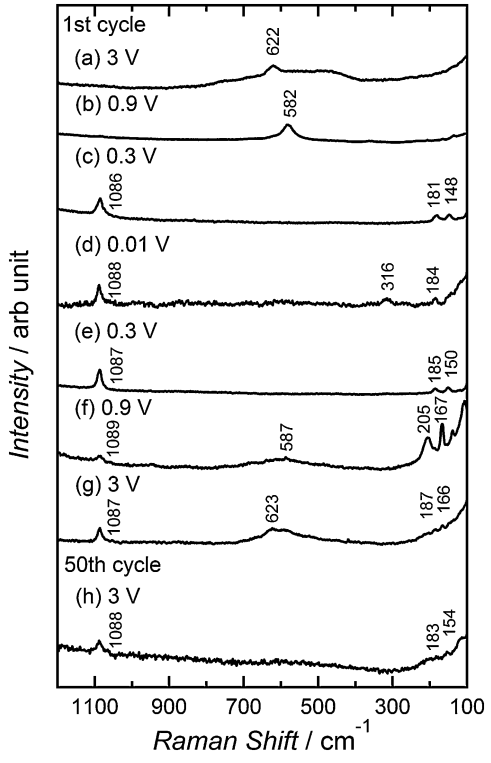

Figure 5. Ex situ micro-Raman spectra of the SnO_2 nanoparticle electrodes at different voltages during the 1st cycle and at the end of 50th cycle. All electrodes were exposed to air before the measurements.

broad peak of $Li_{4.4}Sn$ phase also appeared at the 50th cycle. Courtney et al. reported that irreversible $Li_{4.4}Sn$ phase was developed during charge–discharge repetition,[2] which is consistent with our results of the XRD as well as the cyclic voltammograms.

Figure 5 displays ex situ micro-Raman spectra of the SnO_2 nanoparticle electrodes. Peaks at 622 and 623 cm^{-1} were observed before and after the 1st charge–discharge operation (Figures 5a and 5g). Salis et al. reported that a Raman peak of SnO_2 nanocrystals drifted into lower frequency,[10] whereas that of crystalline SnO_2 is 632 cm^{-1}.[11] The observed peaks corresponded to that of SnO_2 nanocrystals.[10] Peaks at 582 and 587 cm^{-1} were also detected at 0.9 V (Figures 5b and 5f), which were empirically known to correspond to the surface phonon mode from SnO_2 nanoparticles.[12]

Ex situ micro-Raman spectra showed that the SnO_2 spectra completely disappeared under the 1st lithium insertion and reappeared after the 1st deinsertion. This finding indicates that SnO_2 was reduced to Sn metal because bonding states of metal cannot be detected by typical Raman spectroscopy.

Peaks at around 150, 180, 320, and 1088 cm^{-1} were also observed during the 1st charge–discharge cycle and at the end of 50th cycle, which corresponded to those of Li_2O and Li_2CO_3.[13,14] The Li_2O was generated by the redox reactions,[9] and the Li_2CO_3 would be formed by carbonation of Li_2O because the electrodes were exposed to air before the measurements.

The charge–discharge reactions of the commercial SnO_2 products were mostly caused by the Li–Sn alloying–dealloying reactions after the initial lithium insertion.[1] On the other hand, the micro-Raman spectroscopy, X-ray diffraction, and cyclic voltammetry studies of the microwave-synthesized SnO_2 nanoparticles showed that the lithium insertion–deinsertion reactions at early cycles were caused by both redox of SnO_2 and Li–Sn alloying–dealloying reactions, whereas only the alloying–dealloying reactions took place at the 50th cycle. The redox ability at early cycles would be enhanced by the smallness of SnO_2 synthesized by the microwave heating.

Although the cycle performance of SnO_2 could be improved by the smallness and uniformity of the active material, the capacity retention is still in problem. The alloying–dealloying reaction was partly irreversible because of the development of $Li_{4.4}Sn$ phase, and the redox ability of the SnO_2 nanoparticles was gradually lost during the charge–discharge repetition. Thus, degradation of the cycle performance can be explained by depression of redox ability of the SnO_2 nanoparticles at early cycles and development of the irreversible $Li_{4.4}Sn$ phase at later cycles.

The alloying–dealloying of Sn contributes to the rechargeable capacity except for the early charge–discharge stage. The capacity at the 50th cycle was considerably close to the theoretical capacity of the alloying–dealloying reaction (782 mA h g^{-1}). The utilization fraction of Sn metal was calculated to be 82% during the alloying–dealloying reaction at the 50th cycle. This finding indicates that degradation of the cycle performance is mainly attributable to depression of redox ability of the SnO_2 nanoparticles. In the future work, it is necessary to find the mechanism of maintaining the redox ability of SnO_2 during charge–discharge repetition.

This work was financially supported by the New Energy and Industrial Technology Development Organization (NEDO) in Japan. A part of this work was conducted at the Nano-Processing Facility, supported by IBEC Innovation Platform, AIST.

References and Notes

† Present address: Tokai University, 4-1-1 Kitakaname, Hiratsuka, Kanagawa 259-1292
1 Y. Idota, T. Kubota, A. Matsufuji, Y. Maekawa, T. Miyasaka, *Science* **1997**, *276*, 1395.
2 I. A. Courtney, J. R. Dahn, *J. Electrochem. Soc.* **1997**, *144*, 2045.
3 J.-H. Kim, G.-J. Jeong, Y.-W. Kim, H.-J. Sohn, C. W. Park, C. K. Lee, *J. Electrochem. Soc.* **2003**, *150*, A1544.
4 M. Yoshinaga, N. Kijima, S. Wakahara, J. Akimoto, *Chem. Lett.* **2011**, *40*, 414.
5 M. Yoshinaga, N. Kijima, S. Wakahara, J. Akimoto, *Key Eng. Mater.* **2011**, *485*, 127.
6 N. Kijima, Y. Takahashi, H. Hayakawa, J. Awaka, J. Akimoto, *Chem. Lett.* **2007**, *36*, 568.
7 N. Kijima, M. Yoshinaga, J. Awaka, J. Akimoto, *Solid State Ionics* **2011**, *192*, 293.
8 V. Subramanian, W. W. Burke, H. Zhu, B. Wei, *J. Phys. Chem. C* **2008**, *112*, 4550.
9 J. Xie, N. Imanishi, A. Hirano, Y. Takeda, O. Yamamoto, X. B. Zhao, G. S. Cao, *Solid State Ionics* **2010**, *181*, 1611.
10 M. Salis, P. C. Ricci, G. Cappelletti, A. Anedda, *Chem. Phys. Lett.* **2010**, *496*, 109.
11 J. F. Scott, *J. Chem. Phys.* **1970**, *53*, 852.
12 J. Zuo, C. Xu, X. Liu, C. Wang, C. Wang, Y. Hu, Y. Qian, *J. Appl. Phys.* **1994**, *75*, 1835.
13 W. H. Ho, H. C. Liu, H. C. Chen, S. K. Yen, *Surf. Coat. Technol.* **2007**, *201*, 7100.
14 M. H. Brooker, J. B. Bates, *J. Chem. Phys.* **1971**, *54*, 4788.

